Dissociation of the ground state vinoxy radical and its photolytic precursor chloroacetaldehyde: Electronic nonadiabaticity and the suppression of the H+ketene channel

Johanna L. Miller, Laura R. McCunn, Maria J. Krisch, and Laurie J. Butler[a)]
The James Franck Institute and The Department of Chemistry, The University of Chicago, Chicago, Illinois 60637

Jinian Shu
Chemical Sciences Division, Lawrence Berkeley National Laboratory, Berkeley, California 94720

(Received 24 March 2004; accepted 4 May 2004)

This work is a study of the competition between the two unimolecular reaction channels available to the vinoxy radical (CH_2CHO), C—H fission to form H+ketene, and isomerization to the acetyl radical (CH_3CO) followed by C—C fission to form CH_3+CO. Chloroacetaldehyde (CH_2ClCHO) was used as a photolytic precursor to the vinoxy radical in its ground state; photodissociation of chloroacetaldehyde at 193 nm produces vinoxy radicals with internal energies spanning the G3//B3LYP calculated barriers to the two available unimolecular reaction channels. The onset of the CH_3+CO channel, via isomerization to the acetyl radical, was found to occur at an internal energy of 41 ± 2 kcal/mol, agreeing well with our calculated isomerization barrier of 40.8 kcal/mol. Branching to the H+ketene channel was too small to be detected; we conclude that the branching to the H+ketene channel must be at least a factor of 200 lower than what is predicted by a RRKM analysis based on our electronic structure calculations. This dramatic result may be explained in part by the presence of a conical intersection at planar geometries along the reaction coordinate leading to H+ketene, which results in electronically nonadiabatic recrossing of the transition state.
 [DOI: 10.1063/1.1765653]

I. INTRODUCTION

The vinoxy radical, CH_2CHO, is a species of great interest, both theoretically and practically. From a practical standpoint, it plays an important role as an intermediate in combustion reactions. CH_2CHO is known to be a product of the reactions $O(^3P)+C_2H_4$,[1] $O(^3P)+C_2H_3$,[2] $OH+C_2H_2$,[3] and $OH+C_2H_4O$.[4] Because these reactions all involve species that are present in the combustion of larger hydrocarbons,[5,6] the dissociation dynamics of the vinoxy radical are of considerable importance in gaining an understanding of hydrocarbon combustion chemistry.

From a theoretical perspective, the vinoxy radical serves as a means to test our ability to use first-principle quantum mechanics to predict chemical reaction rates and product branching. The branching ratio between the two dissociation channels of the vinoxy radical,

$$CH_2CHO \rightarrow H_2C{=}C{=}O \text{ (ketene)} + H, \quad (1)$$

$$CH_2CHO \rightarrow CH_3CO \text{ (acetyl radical)} \rightarrow CH_3 + CO, \quad (2)$$

was investigated in prior work by Osborn *et al.*[7] In their study, vinoxy radicals were generated by laser photodetachment of the CH_2CHO^- anion, and photoexcited to the $\tilde{B}(^2A'')$ state. They observed that the H+ketene channel dominated the CH_3+CO channel, with a branching ratio of approximately 4 ± 2:1. They interpreted their results as being consistent with internal conversion to the $\tilde{X}(^2A'')$ state followed by dissociation on the ground state potential energy surface. Matsika and Yarkony[8] found that there is an avoided crossing between the $\tilde{B}(^2A'')$ and $\tilde{A}(^2A')$ states, and a conical intersection between the $\tilde{A}(^2A')$ and $\tilde{X}(^2A'')$ states, that could facilitate internal conversion from the $\tilde{B}(^2A'')$ state to the ground state.

At planar geometries, a vinoxy radical undergoing C—H fission to form H+ketene encounters a conical intersection.[7,9] That is, the *p* orbital containing the unpaired electron (in the ground state) on the terminal C atom is perpendicular to the radical orbital being formed on the central C atom by the breaking of the C—H bond. In planar geometry, the two radical orbitals, one a' and the other a'', cannot interact to contribute to a π bonding orbital so the ground state of the vinoxy radical correlates diabatically to the triplet state of ketene, which is energetically inaccessible. Therefore, one anticipates a considerable probability that a dissociative trajectory heading toward H+ketene will undergo an electronically nonadiabatic recrossing of the transition state.[10] This would reduce the branching to the H+ketene product channel compared to the product branching predicted by any method which incorporates the Born-Oppenheimer approximation, including statistical transition state theories as well as exact quantum reactive scattering calculations on a single adiabatic potential energy surface. Though Osborn *et al.* found, in their study, a product branching ratio in rough agreement with their RRKM calculations,

a)Author to whom correspondence should be addressed. Electronic mail: L-Butler@uchicago.edu

we decided to investigate the system further, to elucidate the effect of electronic nonadiabaticity on the product branching. In the Osborn work, the vinoxy radical was produced in the $\tilde{B}(^2A'')$ electronic state, from which internal conversion to the ground state and subsequent dissociation on the ground state surface was assumed to be the mechanism. In contrast, our experimental method produces the vinoxy radical directly in the ground state.

In the past, alkyl vinyl ethers have been commonly used as precursors to the vinoxy radical. Morton, Szpunar, and Butler[11] have found that methyl vinyl ether photodissociated at 193 nm produces vinoxy radicals mostly in the excited $\tilde{A}(^2A')$ electronic state. This is consistent with electronic propensity rules for electronically diabatic dissociation dynamics, in that the $\tilde{A}$ state of the vinoxy radical has the unpaired electron density centered on the oxygen atom in an a' orbital, while the $\tilde{X}(^2A'')$ state has the unpaired electron density centered on the terminal carbon atom in an a'' orbital. In the homolytic cleavage of the methyl C—O bond of methyl vinyl ether, the radical electron density remains localized on the oxygen atom of the nascent vinoxy radical.

In this work, we use chloroacetaldehyde ($CH_2Cl—CH{=}O$) as a precursor to the vinoxy radical. The electronic propensity rules suggest that the nascent vinoxy radicals should be produced mostly in the $\tilde{X}$ state. The branching ratio between the ensuing dissociation channels of the nascent vinoxy radicals allows for an evaluation of the validity of the Born-Oppenheimer approximation on the ground state potential energy surface. By comparing our results with those of studies in which the vinoxy radical is produced in an excited electronic state, we may also test the hypothesis (as used, e.g., by Osborn *et al.*) that excited state vinoxy radicals proceed efficiently to the ground state via internal conversion.

II. EXPERIMENT

All data presented here were collected at Endstation 1 of the Chemical Dynamics Beamline (9.0.2) of the Advanced Light Source (ALS) at Lawrence Berkeley National Laboratories. We produced the vinoxy radicals in their ground state from the photodissociation of chloroacetaldehyde (CH_2ClCHO) at 193 nm. The experimental method has been described in detail elsewhere,[12,13] so we provide a summary here. Chloroacetaldehyde was obtained commercially as a 50% solution in water, and used without further purification. The molecular beam of 5% chloroacetaldehyde seeded in helium was expanded through a room temperature pulsed nozzle with an orifice 1 mm in diameter, and subsequently skimmed. The measured velocity distribution of the chloroacetaldehyde beam peaked at 1.8×10^5 cm/s with a full width at half maximum of 21%.

The chloroacetaldehyde molecules were photodissociated using the unpolarized 193 nm output of a Lambda Physik excimer laser operating at the ArF transition. (The laser light was unpolarized in the plane of the source and the detector, leading to a slight preference for detecting photofragments with a positive anisotropy parameter.) The laser power was approximately 50 mJ/pulse throughout the experiment, and the laser beam was focused to an 8 mm^2 spot in the interaction region of the apparatus. The pulsed nozzle frequency was kept constant at 100 Hz, and the laser was operated at either 100 or 50 Hz, depending on whether shot-to-shot background subtraction was used.

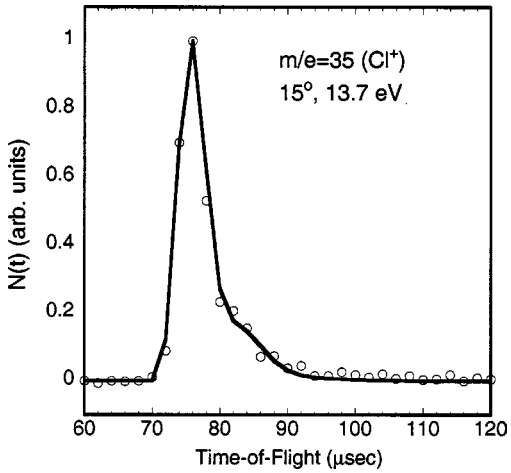

FIG. 1. Time-of-flight spectrum taken at $m/e=35\,(Cl^+)$, with a source angle of 15°, a photoionization energy of 13.7 eV, and an undulator gap of 31.50 mm. The integrated signal was 0.0095 counts per laser shot, over a total of 180 000 laser shots. Data points are shown in open circles. The forward convolution fit shown in the solid line is from the energy distribution shown in Fig. 2.

Photofragments reaching the detector were ionized by the tunable vacuum ultraviolet radiation of the ALS, and filtered by mass-to-charge ratio with a quadrupole. The time-of-flight (TOF) spectra of the mass-selected photofragments included both the flight time of the neutral species through the 15.2 cm flight path from the interaction region to the detector, and the ion flight time through the mass spectrometer, with an ion flight time constant of 5.75 $\mu s/amu^{1/2}$. From the TOF spectra, we then determined the velocity distributions of the mass-selected photofragments.

The nominal photoionization energies of most of the data reported here were calculated using the original beamline calculator at the ALS, prior to a late 2002 recalibration of the light source. It is now known that these photoionization energy values are about 0.20–0.35 eV to the blue of the actual peak energy of the photoionization source. Throughout this work, the photoionization energies we report are the corrected values that take the recalibration into account.

III. RESULTS AND ANALYSIS

A. Primary photodissociation channels of chloroacetaldehyde

We observed two primary dissociation channels of chloroacetaldehyde. The major channel, C—Cl fission to give Cl plus vinoxy, is characterized by the TOF spectrum at $m/e=35\,(Cl^+)$, shown in Fig. 1. The translational energy distribution $[P(E_T)]$ for C–Cl fission was derived from the forward convolution fitting of this spectrum and is shown in Fig. 2. The minor channel, HCl elimination to form HCl plus ketene, is characterized by the TOF spectrum at $m/e=36\,(HCl^+)$, shown in Fig. 3. The corresponding $P(E_T)$

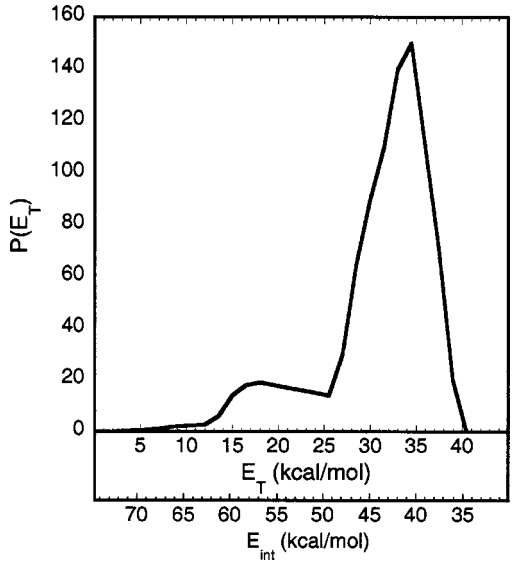

FIG. 2. Translational energy distribution, $P(E_T)$, derived from the forward convolution fit to the Cl^+ spectrum shown in Fig. 1. The upper axis, E_T, is the total kinetic energy of the momentum-matched fragments, Cl and vinoxy. The lower axis, E_{int}, is the corresponding internal energy of the vinoxy radicals.

derived from the fitting of this spectrum is shown in Fig. 4. Although we did not measure the photofragment anisotropy, we expect both channels to be close to isotropic based on results from other analogous systems.

The internal energy, $E_{\text{int}}(\text{vinoxy})$, of the nascent vinoxy radicals may be found using conservation of energy,

$$h\nu + E_{\text{int}}(\text{caa}) = D_0(\text{C—Cl}) + E_T + E_{\text{int}}(\text{vinoxy}) + E_{\text{int}}(\text{Cl}). \tag{3}$$

Here, $h\nu = 148.0$ kcal/mol, the energy of a 193.3 nm photon. $E_{\text{int}}(\text{caa})$ is the internal vibrational energy of the parent chloroacetaldehyde molecules, which is approximately equal to the total internal energy, due to cooling of the molecular rotations in the expansion of the beam. Assuming that the vibrational temperature of the beam is closely approximated by the temperature of the nozzle (25 °C), and using vibrational frequencies calculated at the B3LYP/6-31G(*d*) level and scaled by 0.96,[14] we find the mean value of $E_{\text{int}}(\text{caa})$ to be 1.2 kcal/mol. From calculations using the G3//B3LYP method,[15] we find $D_0(\text{C—Cl})$, the carbon-chlorine bond dissociation energy, to be 74.2 kcal/mol. The internal energy of the chlorine atom, $E_{\text{int}}(\text{Cl})$, is either 0 or 2.5 kcal/mol, for chlorine atoms in the ground and excited spin-orbit states, respectively. Because the spin-orbit splitting is close to the energy resolution of our experiment, and because it is not possible for us to distinguish between the two spin-orbit states of chlorine here, we take $E_{\text{int}}(CL)$ to be zero throughout. Therefore,

$$E_{\text{int}}(\text{vinoxy}) = 75.0 \text{ kcal/mol} - E_T. \tag{4}$$

The translational energy of the C—Cl bond fission events ranges from 4.5 to 40.5 kcal/mol, so $E_{\text{int}}(\text{vinoxy})$ (henceforth, simply E_{int}), ranges from 34.5 to 70.5 kcal/mol, with the majority of vinoxy radicals having internal energies of less than 50 kcal/mol. This range spans the calculated barriers to dissociation of the nascent vinoxy radicals, shown in Fig. 5 and discussed further in Sec. III C.

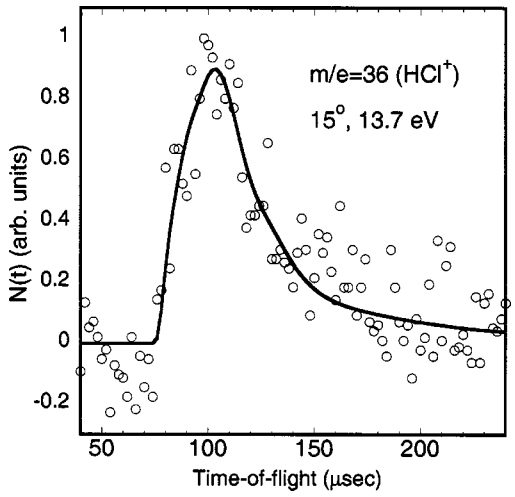

FIG. 3. Time-of-flight spectrum taken at $m/e = 36\,(\text{HCl}^+)$, with a source angle of 15°, a photoionization energy of 13.7 eV, and an undulator gap of 31.50 mm, integrated over a total of 1.8×10^6 laser shots. The $P(E_T)$ derived from the forward convolution fit is shown in Fig. 4.

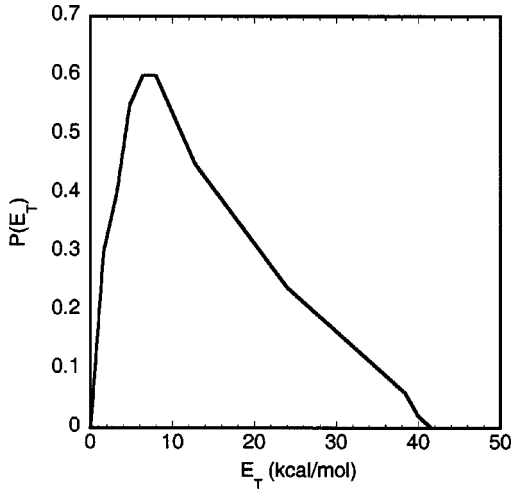

FIG. 4. Translational energy distribution, $P(E_T)$, derived from the forward convolution fit to the HCl^+ spectrum shown in Fig. 3.

We may calculate the branching ratio R between the C—Cl fission and HCl elimination channels using the following equation:

$$R = \frac{N_{\text{Cl}^+}}{N_{\text{HCl}^+}} \frac{\text{TS}_{\text{Cl}^+}}{\text{TS}_{\text{HCl}^+}} \frac{Q_{\text{HCl}}}{Q_{\text{Cl}}} \frac{f_{\text{HCl}}}{f_{\text{Cl}}}, \tag{5}$$

where N_x is the integrated, background-subtracted signal of species x, normalized for the number of laser shots; TS_x is the theoretical scaling factor, which accounts for the Jacobian factors in the analysis of the TOF spectra and the greater sensitivity to fragments with longer transit times through the ionization region; Q_x is the photoionization cross section of species x; f_x is the fraction of the ionized fragments of species x that do not undergo dissociative ionization.

To obtain N_{HCl^+}, we integrate the HCl spectrum shown in Fig. 3 (which was collected over 1.8×10^6 laser shots),

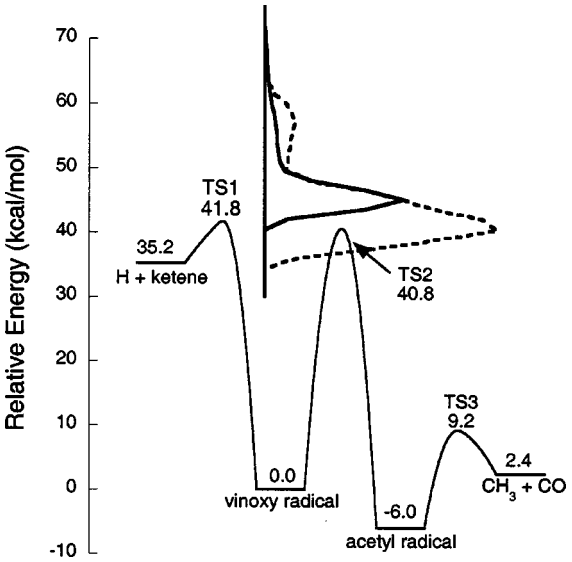

FIG. 5. G3//B3LYP calculated energies of the relevant species involved in the unimolecular dissociation of the vinoxy radical. All energies include zero-point energy, and are relative to the ground state of the vinoxy radical. Superimposed on the potential energy diagram is the distribution of internal energies $[P(E_{\text{int}})]$ of the nascent vinoxy radicals (dashed line) and of those vinoxy radicals that isomerize and then dissociate, contributing to the signal at $m/e=15$ (solid line). The onset of the isomerization agrees well with the calculated barrier to isomerization.

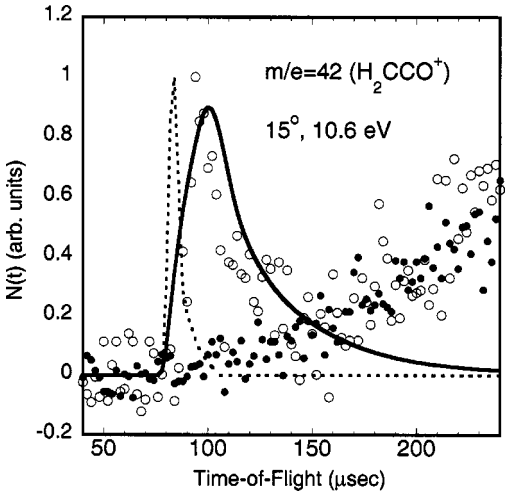

FIG. 6. Time-of-flight spectrum taken at $m/e=42\,(H_2CCO^+)$, with a source angle of 15°, a photoionization energy of 10.6 eV, and an undulator gap of 27.82 mm. A MgF_2 filter was used to eliminate the higher harmonics of the photoionization radiation. The integrated signal was 0.00044 counts per laser shot. Data points are shown in open circles. Due to time constraints, this spectrum was taken without background subtraction, so we superimpose onto this spectrum the laser-off background from $m/e=15$ in solid circles, corrected for the difference in ion flight times. The solid line is the forward convolution fit calculated from the HCl elimination $P(E_T)$ shown in Fig. 4 and derived from the $m/e=36$ spectrum shown in Fig. 3. The dotted line is calculated from the $m/e=35$ $p(E_T)$ shown in Fig. 2, and represents the range of arrival times at which ketene product from the unimolecular dissociation of vinoxy radicals should be observed.

from 74 to 196 μs and subtract the average background of 129.4 counts per channel. To obtain N_{Cl^+}, we integrate a spectrum not shown here (which was collected over 600 000 laser shots on the same day as the $m/e=36$ spectrum) from 76 to 100 μs and subtract the average background of 4.5 counts per channel. This $m/e=35$ spectrum was collected in short blocks, alternating with the $m/e=36$ spectrum, so it is not necessary to account for changes in laser power or photoionization power, as these factors should have the same effect on both spectra.

The theoretical scaling factors were computed using a forward convolution fitting program. The ionization cross sections were taken from the literature.[16,17] Because Cl is an atom and can have no daughter ions, $f_{Cl}=1$, and we assume that $f_{HCl}=1$ as well. Thus, we have

$$R=\frac{5987/6}{2486/18}\times\frac{61.68}{20.77}\times\frac{56}{43.6}\times\frac{1}{1}=27.14. \quad (6)$$

B. Unimolecular dissociation channels of the vinoxy radical

1. C—H fission to form H+ketene

Signal of a very small magnitude was observed at $m/e=42\,(H_2CCO^+)$, shown in the TOF spectrum in Fig. 6. The dashed line in Fig. 6, however, represents the expected time of flight of ketene molecules produced via C—H fission of vinoxy radicals, momentum-matched to the $m/e=35$ spectrum of Fig. 1. (Since C—H fission imparts little recoil velocity to the ketene product, the translational energies of the ketene fragments may be approximated by the translational energies of the vinoxy radicals from which they were formed.) There is no apparent signal at this range of arrival times, so the observed ketene signal cannot be from the dissociation of vinoxy radicals. The solid line, on the other hand, represents the expected time of flight of ketene molecules produced via the minor HCl elimination channel from the photolytic precursor chloroacetaldehyde, momentum-matched to the $m/e=36$ spectrum of Fig. 3. This is a good fit to the data. Therefore, the vinoxy radicals that result from photodissociation of chloroacetaldehyde at 193 nm undergo no detectable C—H fission, despite this being reported as the major dissociation channel by Osborn *et al.* This point is addressed more quantitatively in the Discussion.

The HCl elimination $P(E_T)$ does slightly overfit the slow side of the $m/e=42$ spectrum; this may be due to secondary dissociation of ketene. Two dissociation channels, H+HCCO and CH_2+CO, are energetically accessible to the ketene products of HCl elimination.[18] Due to the poor signal-to-noise level in our $m/e=42$ spectrum, we do not attempt to characterize the portion of the ketene products of HCl elimination that undergo secondary dissociation. However, we note that none of the possible ketene dissociation products has a mass that could contribute to any of the spectra we consider here. Also note that if vinoxy radicals underwent C—H fission to form H+ketene, those ketene products should be detected at $m/e=42$, as they have little internal energy.

2. Isomerization to acetyl followed by C—C fission to form CH_3+CO

Figure 7 depicts the TOF spectrum taken at $m/e=15$, corresponding to methyl radical products of the other unimo-

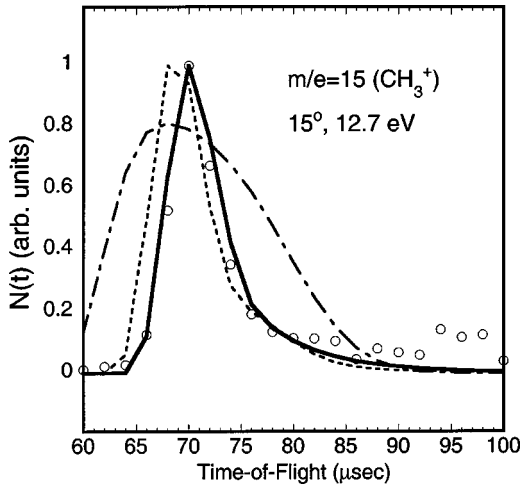

FIG. 7. Time-of-flight spectrum taken at $m/e=15\,(CH_3^+)$, with a source angle of 15°, a photoionization energy of 12.7 eV, and an undulator gap of 30.45 mm. The solid line is the forward convolution fit calculated from the $P(E_T)$ in Fig. 8, assuming that the observed methyl radicals result from unimolecular dissociation of acetyl radicals, with negligible kinetic energy imparted to the nascent products. The dotted line is the unsatisfactory fit calculated from the entire $m/e=35\,P(E_T)$, shown in Fig. 2. The dashed-dotted line is the unsatisfactory fit obtained under the assumption that secondary dissociation of the acetyl radical imparts 1.0 kcal/mol of translational energy to the methyl and CO products.

lecular dissociation channel, isomerization to acetyl followed by C—C bond fission to yield CH_3+CO. This spectrum is well fit by a subdistribution of the C—Cl fission $P(E_T)$, shown in Fig. 8. Figure 5 shows the C—Cl fission $P(E_T)$ superimposed on a diagram of the energies of the calculated transition states. The part of the $P(E_T)$ that fits the $m/e=15$ spectrum results only from vinoxy radicals with more than about 41 kcal/mol of internal energy, consistent with the calculated barrier height for isomerization to the acetyl radical. (The deviation of the $m/e=15\,P(E_T)$ from the $m/e=35\,P(E_T)$ at higher internal energies may be due to the presence of clusters.) Surprisingly, this fit implies that the C—C bond fission of the acetyl radical imparts negligible recoil velocity to the nascent CH_3 and CO products.

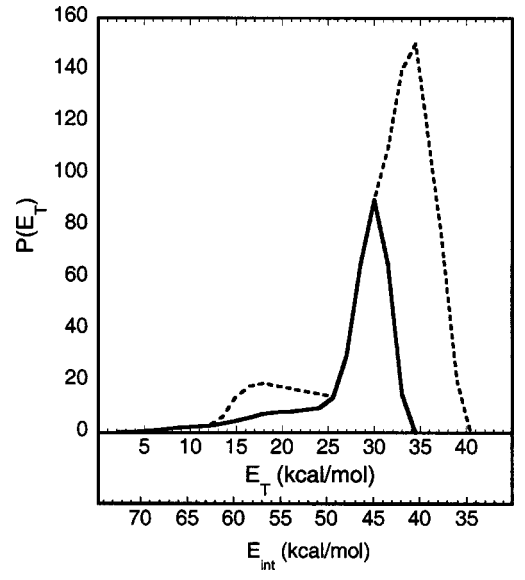

FIG. 8. The solid line is the translational energy distribution, $P(E_T)$, derived from the forward convolution fit to the CH_3^+ spectrum shown in Fig. 7. The upper axis, E_T, is the translational energy imparted to the vinoxy and Cl products of the initial dissociation of chloroacetaldehyde; the lower axis, E_{int}, is the internal energy of the vinoxy radicals. This $P(E_T)$ corresponds to those vinoxy radicals with enough internal energy to isomerize to acetyl radicals, and subsequently dissociate into methyl and CO products. The dotted line is the entire primary $P(E_T)$, also shown in Fig. 2.

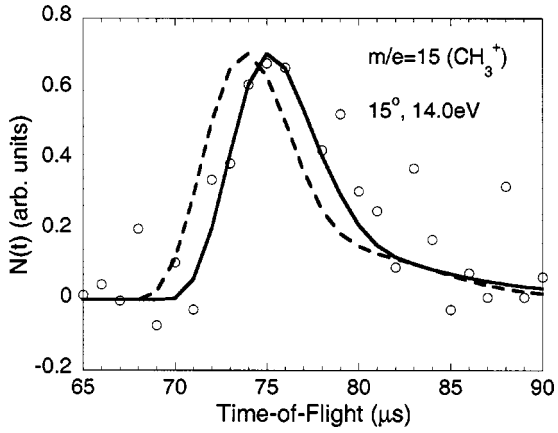

FIG. 9. Time-of-flight spectrum taken at $m/e=15\,(CH_3^+)$, with a source angle of 15° and a photoionization energy of 14.0 eV. Data points are shown in open circles. The solid line is the forward convolution fit to the data using the same $P(E_T)$ as was used to fit the spectrum in Fig. 7. The dashed line is the unsatisfactory forward convolution fit calculated from the entire C—Cl fission $P(E_T)$. This spectrum was taken using a quadrupole with a different ion flight time constant than the one used to obtain the Fig. 7 spectrum, so although the absolute time of arrival of the photofragments differs between the two spectra, they are both well fit by the same $P(E_T)$.

For comparison, Fig. 7 also depicts two unsatisfactory forward convolution fits. The dashed-dotted line is the best fit that could be obtained by assuming that the C—C bond fission of the acetyl radical imparts just 1.0 kcal/mol of translational energy to the nascent products; that this fit is far too broad supports the conclusion that the recoil velocity from secondary dissociation is indeed negligible. The dotted line is the fit calculated using the entire C—Cl fission $P(E_T)$; that this fit is significantly too fast supports our assignment of this signal to methyl radical products of unimolecular dissociation of vibrationally excited vinoxy radicals, rather than dissociative ionization of stable vinoxy products.

To further support our conclusion that the $m/e=15$ signal does not result from dissociative ionization, we consider the possibility that dissociative ionization efficiency is strongly dependent on the internal energy of the vinoxy radicals. That is, if the internal vibrational energy of the vinoxy radicals contributes, along with the energy of the ionizing photon, to the energy necessary for dissociative ionization, then only those vinoxy radicals with E_{int} greater than some cutoff would undergo dissociative ionization and be detected at $m/e=15$; this, too, would result in the truncated $P(E_T)$ that fits the Fig. 7 spectrum well. Figure 9 shows a $m/e=15$ spectrum taken with a photoionization energy of 14.0 eV, compared to the 12.7 eV used in the Fig. 7 spectrum. If the $m/e=15$ signal is, in fact, due to dissociative ionization of stable vinoxy radicals, then increasing the photoionization energy should decrease the minimum internal energy necessary for dissociative ionization. If we assume that in-

TABLE I. Vibrational frequencies of species in the C_2H_3O system, calculated at the B3LYP/6-31G (d) level. These frequencies as presented are unscaled, and should be scaled by 0.96.

Species	Unscaled vibrational frequencies (cm^{-1})
Vinoxy	459, 505, 751, 977, 985, 1168, 1416, 1496, 1573, 2965, 3173, 3284
Acetyl	109, 463, 855, 963, 1059, 1382, 1485, 1488, 1939, 3043, 3133, 3137
TS1	792i, 328, 493, 533, 587, 634, 1010, 1151, 1434, 2152, 3196, 3309
TS2	1601i, 429, 635, 851, 1043, 1137, 1250, 1483, 1843, 1901, 3075, 3255
TS3	233i, 11, 225, 455, 459, 780, 1437, 1441, 2109, 3134, 3302, 3304

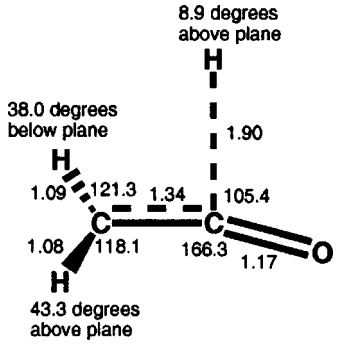

FIG. 10. The calculated structure of the transition state between the vinoxy radical and H+ketene products, optimized at the B3LYP level with the 6-31G (d) basis set. All bond lengths are in angstroms, and all angles are in degrees. All dihedral angles are with respect to the C—C bond.

creasing the photoionization energy by 1.3 eV (30 kcal/mol) decreases this cutoff internal energy by the same amount, then the 14.0 eV spectrum should be well fit by the entire C—Cl fission $P(E_T)$. This is clearly not the case; rather, the fast edge of the 14.0 eV spectrum is best fit by the same truncated $P(E_T)$ that fits the 12.7 eV spectrum. (The poorness of the fit on the slow side may be due to the presence of clusters.) Thus, the $m/e=15$ signal is not due to dissociative ionization of vinoxy radicals.

The onset of this dissociation channel is not perfectly sharp because E_{int} includes both vibrational and rotational energy of the vinoxy radical; the former can contribute to the isomerization to acetyl, while the latter largely cannot. Therefore, our experimental determination of the energy barrier to dissociation is equal to the smallest value of E_{int} for which $m/e=15$ signal is observed, i.e., 41 ± 2 kcal/mol. This is in good agreement with our calculated value of 40.8 ± 2 kcal/mol, presented below.

We were unable to detect any measurable signal corresponding to the CO products of secondary dissociation above the very high background level found at $m/e=28$. We also did not observe signal at any mass corresponding to stable vinoxy radicals or dissociative ionization thereof. While the ionization energy of the vinoxy radical has been calculated to be approximately 9.13 eV,[19] the cation equilibrium geometry is very different from that of the neutral radical, so the Franck-Condon factors are expected to be small up to at least 10.2 eV. No group has yet succeeded in measuring the photoionization spectrum of the vinoxy radical, although vinoxy radical products have been reported in reactive scattering experiments using low-energy electron bombardment detection.[20]

C. Electronic structure calculations

To assist in the intepretation of our results, we have performed electronic structure calculations of the energies, geometries, and vibrational frequencies of some relevant species on the C_2H_3O potential energy surface. For all calculations, we used the GAUSSIAN 98 program, revision A.11.3 (Ref. 21) and the G3//B3LYP method.[15] Our calculated values for the relative zero-point corrected energies of these species are shown in Fig. 5, and our calculated (unscaled) frequencies are given in Table I.

For the most part, our results are in good agreement with those presented by Osborn *et al.*[7] in Fig. 8 of their work. The one exception is the energy barrier to the C—H fission of the vinoxy radical, producing H+ketene. We found this barrier to be 41.8 kcal/mol, compared to the value reported in Osborn *et al.* of 37.6 kcal/mol. The reason for this discrepancy is that the value reported in Osborn *et al.* is not based on an actual transition state structure, but is an estimation based on an analogy proposed by Benson,[22] whereas our value is the G3//B3LYP energy of the B3LYP/6-31G (d) optimized transition state structure shown in Fig. 10.

IV. DISCUSSION

A. Assignment of the nascent vinoxy electronic state

Electronic propensity suggests that photolysis of chloroacetaldehyde ought to produce vinoxy radicals in the $\tilde{X}(^2A'')$ state, in which the radical electron is localized on the terminal C atom, rather than in the $\tilde{A}(^2A')$ state, in which the unpaired electron is localized on the O atom. (The $\tilde{B}$ state, which lies more than 80 kcal/mol above the $\tilde{X}$ state, is energetically inaccessible, but the $\tilde{A}$ state, which lies only 23 kcal/mol above the $\tilde{X}$ state, cannot be ruled out on the basis of energetics alone.) We are able to confirm our assignment of the $\tilde{X}$ state to the nascent vinoxy radicals by comparing our experimental observations with the results of the photodissociation of methyl vinyl ether. Morton, Szpunar, and Butler[11] found that the photodissociation of methyl vinyl ether produces the vinoxy radical with a bimodal $P(E_T)$. Those authors assigned the peak at high translational energies to the $\tilde{X}$ state, and the peak at lower translational energies to the $\tilde{A}$ state, based on the observation that vinoxy radicals in the two peaks exhibited different cracking patterns to $m/e=14$ and $m/e=15$. (Morton *et al.* used electron impact ionization, rather than photoionization, in their experiment, so the photofragments underwent dissociative ionization to a greater degree than did the photofragments we observed here.) They concluded that the $\tilde{A}$ state radicals were produced with between 42 and 86 kcal/mol of internal energy (including the 23 kcal/mol of electronic energy to account for the difference in energy between the $\tilde{X}$ state and the $\tilde{A}$ state) and that a large fraction of them underwent C—H fission to yield H+ketene. Because our experiment

TABLE II. Predicted branching to the two unimolecular reaction channels available to the ground state vinoxy radical (C—H fission to form H+ketene, and isomerization to acetyl followed by C—C fission to form CH_3 +CO), as a function of internal energy, calculated via RRKM. To obtain the first set of branching ratios, we used the barrier heights and scaled vibrational frequencies that resulted from our G3//B3LYP calculations. The second set of branching ratios uses a set of adjusted parameters designed to determine the smallest possible branching to the C—H fission channel that would still be consistent with our G3//B3LYP results (see text).

	G3//B3LYP calculated parameters		Adjusted parameters	
E_{int} (kcal/mol)	C—H fission	Isomerization	C—H fission	Isomerization
42.0	27.5	72.5	0.0	100.0
45.0	59.0	41.0	7.5	92.5
48.0	69.6	30.4	20.7	79.3
51.0	75.2	24.7	32.1	67.9
54.0	78.6	21.4	41.0	59.0
57.0	81.0	19.0	47.9	52.1
60.0	82.7	17.3	53.3	46.7
63.0	84.0	16.0	57.5	42.5
66.0	85.0	15.0	60.9	39.1
69.0	85.8	14.2	63.7	36.3
72.0	86.5	13.5	66.0	34.0
75.0	87.1	12.9	68.0	32.0

produces vinoxy radicals with a similar range of internal energies, and we observe no ketene at all due to C—H fission of vinoxy, we conclude that the photolysis of chloroacetaldehyde produces vinoxy radicals predominantly in the $\tilde{X}$ state.

B. Degree of suppression of the H+ketene channel

In this section, we calculate the magnitude of the signal we would expect to see at $m/e=42$ according to RRKM[23] predictions of the branching between the two unimolecular reaction channels available to the vinoxy radical, compared to the magnitude of the signal we observe due to HCl elimination. This allows us to obtain an upper limit for the branching to H+ketene that could be detected with our signal-to-noise levels, assuming that ketene which results from HCl elimination from the precursor and ketene from the possible C—H fission dissociation channel of vinoxy have similar photoionization cross sections at 10.6 eV.

In a previous section, we found that the branching ratio between the C—Cl fission and HCl elimination channels was approximately 27:1. Accounting for the appropriate theoretical scaling factors (38.43 and 15.40 for the C—Cl fission and HCl elimination distributions, respectively), we find that if we make the unrealistic suppositions that all nascent vinoxy radicals undergo C—H fission to form ketene, and none of the ketene products of HCl elimination undergo secondary dissociation, then the integrated signal of ''fast'' ketene (from vinoxy) should be about 10.9 times that of ''slow'' ketene (from HCl elimination). In this instance, however, the total integrated signal is not the most meaningful measure of the magnitude of a peak. A broad peak, with signal spread over many channels, is much more easily obscured by background noise than is a sharp peak with the same integrated signal. Since we seek to determine the maximum possible fast ketene signal that could be present in our $m/e=42$ spectrum, we will also compare peak heights, as well as areas.

The predicted fast ketene peak, the dotted line in Fig. 6, has 26.2% of its total signal in the peak channel. The slow ketene peak, on the other hand, is much broader, with only 4.4% of its total signal in the peak channel. Therefore, if all of the nascent vinoxy radicals underwent C—H fission to form H+ketene, this would result in a peak, in the location of the dotted line in Fig. 6, that is 64.6 times the height of the slow ketene peak that we do observe. This assumes that ketene from both sources would have the same photoionization efficiency at 10.6 eV. (If the magnitude of the observed ketene peak from HCl elimination is significantly reduced due to ketene dissociation, this only increases the magnitude of the predicted vinoxy dissociation peak. Also note that any anisotropy in the dissociation of the chloroacetaldehyde precursor affects both vinoxy dissociation channels equally, so it is not necessary to take into account in this analysis.) Obviously, we do not see such a peak; however, the assumption of unit quantum yield at $m/e=42$ is not realistic. It is necessary to account for the branching to the CH_3+CO channel, as well as the vinoxy radicals that do not dissociate at all.

We calculate the RRKM branching ratio between the two dissociation channels in two different ways. The first calculation uses the barrier heights and frequencies directly from our G3//B3LYP calculations, as presented in Fig. 5 and Table I. The second is a ''worst case scenario'' calculation, designed to determine the smallest possible branching to H+ketene that would still be consistent with both the assumption of adiabaticity and our G3//B3LYP calculations. For this calculation, we take the barrier to C—H fission to be 43.8 kcal/mol (2.0 kcal/mol higher than our G3//B3LYP value, corresponding to the uncertainty in the calculated energy) and the barrier to isomerization to be 40.0 kcal/mol (0.8 kcal/mol lower, so as to remain consistent with our experimental value.) Also, in this calculation, for the C—H fission transition state only, we replace the vibrational frequencies calculated at the B3LYP level with those calculated at the HF level (and scaled by 0.8929, as used in the G3 calculation.) Use of the Hartree-Fock frequencies predicts a lower density of states for this transition state, resulting in a smaller branching to the H+ketene channel.

Table II shows the results of these RRKM calculations in

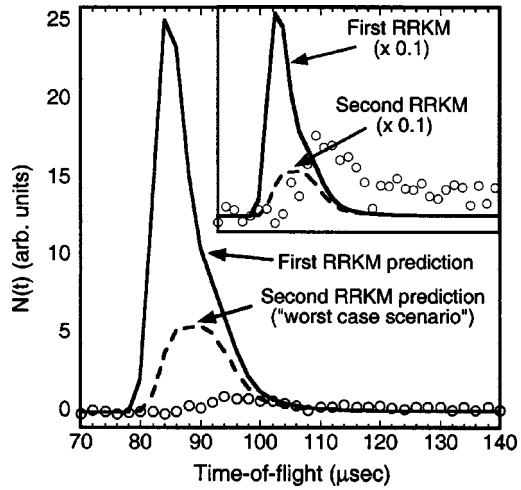

FIG. 11. Two calculated TOF spectra, representing the predicted contribution to the $m/e=42$ signal from C—H fission of the vinoxy radical. The solid line is the spectrum calculated using the first set of RRKM branching ratios in Table II, which use the barrier heights and scaled vibrational frequencies from our G3//B3LYP calculations. The dashed line is the spectrum calculated using the second set of RRKM branching ratios, which use the adjusted "worst case scenario" barrier heights and vibrational frequencies, as described in the text. The observed $m/e=42$ data are shown in open circles. The inset depicts the same spectra, with the RRKM predictions reduced by a factor of 10.

terms of the predicted branching ratio between the two unimolecular dissociation channels of the vinoxy radical, as a function of the internal energy. For both calculations, the branching between the two channels changes substantially over the relevant range of internal energies. Combining the calculated branching ratios with the C—Cl fission $P(E_T)$, we get an overall branching of 4:3 for the first calculation (with H+ketene being the slightly favored channel) and 1:6.6 for the second RRKM calculation (with CH_3+CO being the dominant channel). Figure 11 depicts the predicted C—H fission contributions to the $m/e=42$ spectrum, superimposed on the observed $m/e=42$ data. The inset shows the same predicted spectra reduced by a factor of 10, for ease of comparison with the shape of the observed $m/e=42$ spectrum. Note that even the worst case scenario RRKM calculation predicts a C—H fission peak more than five times the size of the observed HCl elimination peak.

Both RRKM calculated spectra predict substantial signal in the time-of-flight range 84–86 μs, where there is no apparent signal in the observed spectrum. Any actual signal at this range of arrival times would have to be completely obscured by the background noise, in which case its magnitude could be at most about 0.1 times that of the observed peak. Therefore, the branching to the C—H fission channel of the vinoxy radical is suppressed by a factor of at least 50 (using the adjusted RRKM parameters), and possibly more than 200 (using the RRKM parameters directly from our electronic structure calculations). This dramatic suppression of the C—H fission channel is likely due to nonadiabatic recrossing of the transition state and inefficient IVR (intramolecular vibrational energy redistribution) into torsional modes, as detailed in the following section.

V. CONCLUSION

Chloroacetaldehyde, when photodissociated at 193 nm, serves as a precursor to the vinoxy radical. The subsequent reaction dynamics of the nascent vinoxy radicals differ significantly from those observed by both Osborn *et al.*,[7] who photoexcited vinoxy radicals into the $\tilde{B}(^2A'')$ electronic state, and Morton, Szpunar, and Butler,[11] who produced vinoxy radicals primarily in the $\tilde{A}(^2A')$ electronic state via photodissociation of methyl vinyl ether. In both of those studies, a large fraction of the vinoxy radicals underwent C—H fission to form H+ketene, whereas we did not observe this channel at all. From this, we conclude that photodissociation of chloroacetaldehyde yields vinoxy radicals in their ground, or $\tilde{X}(^2A'')$, electronic state, and that internal conversion from the $\tilde{B}$ or $\tilde{A}$ state to the $\tilde{X}$ state may not proceed as efficiently as previously thought. Osborn *et al.*'s observation of H+ketene as the dominant set of dissociation products is consistent with electronically diabatic C—H fission on the $\tilde{A}$ state potential energy surface. Thus, it is possible that the radiationless transition from the $\tilde{B}$ state to the $\tilde{A}$ state proceeds as proposed by Matsika and Yarkony, while the internal conversion to the ground state is not effective.

However, the vinoxy dissociation dynamics we observed are also significantly different from what is predicted by RRKM using the results of our G3//B3LYP calculations of the relevant stationary points on the C_2H_3O potential energy surface. We found that vinoxy radicals with more than 41.0 ± 2 kcal/mol of internal energy isomerize to acetyl, which then dissociates to CH_3+CO; this agrees well with our calculated barrier to this channel. However, the branching to the H+ketene channel was observed to be less than 0.5% of what is predicted by our RRKM calculations.

The suppression of the H+ketene channel may be related to the presence of a conical intersection encountered by dissociative trajectories confined to planar geometries, but the transition state we found between the vinoxy radical and H+ketene in their ground states is highly nonplanar, so dissociative trajectories close to the minimum energy path should bypass the conical intersection. It is possible that the torsional vibrational mode of the vinoxy radical does not couple efficiently to the other vibrational modes, so that the nonplanar transition state is not easily accessible. Future work is necessary, however, to determine whether this explanation is able to entirely account for the observed suppression of the H+ketene channel.

ACKNOWLEDGMENTS

This work was supported by the National Science Foundation under Grant No. CHE-0109588. The Chemical Dynamics Beamline at the ALS was supported by the Director, Office of Science, Office of Basic Energy Sciences, Chemical Sciences Division of the U.S. Department of Energy under Contract No. DE-AC03-76SF00098. The ALS facility was supported by the Director, Office of Science, Office of Basic Energy Sciences, Materials Sciences Division of the U.S. Department of Energy, under the same contract. J.L.M. and M.J.K., respectively, acknowledge the support of DOD and NSF Graduate Fellowships. L.R.M. was supported in

part by a GAANN Fellowship. We acknowledge the Burroughs Wellcome Fund Interfaces Cross-Disciplinary Training Program at the University of Chicago for partial support of the computer cluster used for some of the calculations presented here.

[1] A. M. Schmoltner, P. M. Chu, R. J. Brudzynski, and Y. T. Lee, J. Chem. Phys. **91**, 6926 (1989).
[2] D. J. Donaldson, I. V. Okuda, and J. J. Sloan, Chem. Phys. **193**, 37 (1995).
[3] V. Schmidt, G. Y. Zhu, K. H. Becker, and E. H. Fink, Ber. Bunsenges. Phys. Chem. **89**, 321 (1985).
[4] K. Lorenz and R. Zellner, Ber. Bunsenges. Phys. Chem. **88**, 1228 (1984); T. J. Wallington, R. Liu, P. Dagaut, and M. J. Kurylo, Int. J. Chem. Kinet. **20**, 41 (1988).
[5] C. K. Westbrook and F. L. Dryer, *Eighteenth Symposium (International) on Combustion* (Combustion Institute, Pittsburgh, 1981), p. 749.
[6] K. Brezinsky, Prog. Energy Combust. Sci. **12**, 1 (1986).
[7] D. L. Osborn, H. Choi, D. H. Mordaunt, R. T. Bise, D. M. Neumark, and C. M. Rohlfing, J. Chem. Phys. **106**, 3049 (1997).
[8] S. Matsika and D. R. Yarkony, J. Chem. Phys. **117**, 7198 (2002).
[9] D. R. Yarkony, J. Phys. Chem. A **105**, 6277 (2001).
[10] L. J. Butler, Annu. Rev. Phys. Chem. **49**, 125 (1998), and references therein.
[11] M. L. Morton, D. E. Szpunar, and L. J. Butler, J. Chem. Phys. **115**, 204 (2001).
[12] J. A. Mueller, B. F. Parsons, L. J. Butler, F. Qi, O. Sorkhabi, and A. G. Suits, J. Chem. Phys. **114**, 4505 (2001).
[13] D. E. Szpunar, Y. Liu, M. J. McCullagh, L. J. Butler, and J. Shu, J. Chem. Phys. **119**, 5078 (2003).
[14] A. P. Scott and L. Radom, J. Phys. Chem. **101**, 7119 (1997).
[15] A. G. Baboul, L. A. Curtiss, P. C. Redfern, and K. Raghavachari, J. Chem. Phys. **110**, 7650 (1999).
[16] J. A. R. Samson, Y. Shefer, and G. C. Angel, Phys. Rev. Lett. **56**, 2020 (1986).
[17] J. W. Gallagher, C. E. Brion, J. A. R. Samson, and P. W. Langhoff, J. Phys. Chem. Ref. Data **17**, 9 (1988).
[18] J. P. Cole and G. G. Galint-Kurti, J. Chem. Phys. **119**, 6003 (2003).
[19] B. Ruscic (private communication).
[20] P. Casavecchia (unpublished).
[21] M. J. Frisch, G. W. Trucks, H. B. Schlegel *et al.*, GAUSSIAN 98, Revision A.11.3, Gaussian, Inc., Pittsburgh, PA, 2002.
[22] S. W. Benson, *Thermochemical Kinetics* (Wiley, New York, 1968), pp. 140, 205–207.
[23] W. L. Hase and D. L. Bunker, QCPE 234 (1974).